NANO LETTERS

Letter

pubs.acs.org/NanoLett

Direct, Rapid, and Label-Free Detection of Enzyme–Substrate Interactions in Physiological Buffers Using CMOS-Compatible Nanoribbon Sensors

Luye Mu,[†] Ilia A. Droujinine,[‡] Nitin K. Rajan,[§] Sonya D. Sawtelle,[§] and Mark A. Reed*[,†,§]

[†]Department of Electrical Engineering, Yale University, New Haven, Connecticut 06511, United States

[‡]Department of Genetics, Harvard Medical School, Boston, Massachusetts 02115, United States

[§]Department of Applied Physics, Yale University, New Haven, Connecticut 06511, United States

ABSTRACT: We demonstrate the versatility of Al_2O_3-passivated Si nanowire devices ("nanoribbons") in the analysis of enzyme–substrate interactions via the monitoring of pH change. Our approach is shown to be effective through the detection of urea in phosphate buffered saline (PBS), and penicillinase in PBS and urine, at limits of detection of <200 μM and 0.02 units/mL, respectively. The ability to extract accurate enzyme kinetics and the Michaelis–Menten constant (K_m) from the acetylcholine–acetylcholinesterase reaction is also demonstrated.

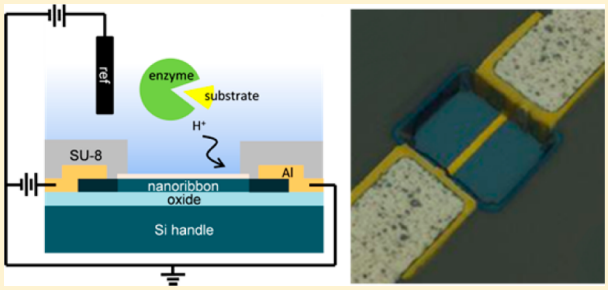

KEYWORDS: *Nanobiosensors, enzyme–substrate interaction, enzyme kinetics, enzyme activity detection, pH sensing*

The need for high-throughput, rapid, and sensitive assessment of enzyme and substrate interaction is of central importance in the fields of clinical diagnosis and treatment, as well as for the discovery of cellular and organismal metabolic regulators. The catalytic activity for enzyme–substrate interactions is an informative measure, as activity within a biological sample is indicative of the functional output of the enzyme and can be more easily related to cellular or organismal phenotype. Current methods of activity detection mostly include colorimetric, fluorometric, chromatographic, and radioactive assays, which either lack sensitivity or require bulky and expensive equipment (e.g., spectrophotometers) and tedious procedures.[1] Many current methods require the use of a labeled substrate, which is not only difficult to synthesize but may alter its interaction with the enzyme. Other methods based on electrochemical assays have also been reported but are typically limited to redox reactions.[2−4]

Many enzymatic reactions release or consume acidic or basic products and thus alter the pH of their environments,[5] suggesting FET-based approaches and a simple, cost-effective method for the detection of these enzymatic reactions. The idea of the enzymatically coupled ion-sensitive field effect transistor (ENFET) was postulated in 1976,[6] and realized in 1979 to detect urea.[7] Since then, various biologically relevant substrates have been detected, such as urea,[8−10] creatinine,[11,12] glucose,[13−15] penicillin,[16,17] and acetylcholine.[18,19]

Prior work focused on the immobilization of enzymes on the surface of the ENFETs, where substrate addition induced a pH change.[16,20] This method cannot be used for enzyme activity quantification, as substrate immobilization is difficult and may render the substrate unrecognizable by the enzyme. In addition, enzyme immobilization presents several significant drawbacks that have hindered the adoption of ENFETs: (1) immobilization may alter the activity of the enzyme compared to its natural environment,[21] which precludes meaningful extraction of kinetic constants; (2) the requirement of device functionalization does not allow for repeated use, introducing device-to-device variability in measurements and significantly increasing cost; (3) functionalizations tend to be unstable in solution with degradation leading to device instabilities over time; and (4) repeatable functionalization of membranes with proteins remains a challenging problem, which leads to issues with reproducibility.

Silicon nanoribbons have been shown to be highly sensitive, low cost pH detectors with superb signal-to-noise ratio[22] and potential for integrated multiplexing. In this Letter, we show that the drawbacks enumerated above can be overcome by combining the enzyme and substrate directly in a small reservoir encasing nonfunctionalized nanoribbons. We use Al_2O_3 as the sensing dielectric surface of the nanoribbon to sensitively, reliably, and stably quantify subtle pH changes in solution. Al_2O_3 is used for numerous reasons: (1) Al_2O_3 has near-Nernstian sensitivity to pH changes;[23,24] (2) Al_2O_3 allows for effective and robust isolation of device channel and solution, preventing leakage current from increasing device noise; (3) the dielectric is a high density material with a low hydration rate, which prevents device drift and dielectric breakdown due to ion incorporation;[25] and (4) Al_2O_3 is feebly charged at neutral pH, therefore reducing fouling due to nonspecific

Received: June 24, 2014
Revised: August 20, 2014
Published: August 28, 2014

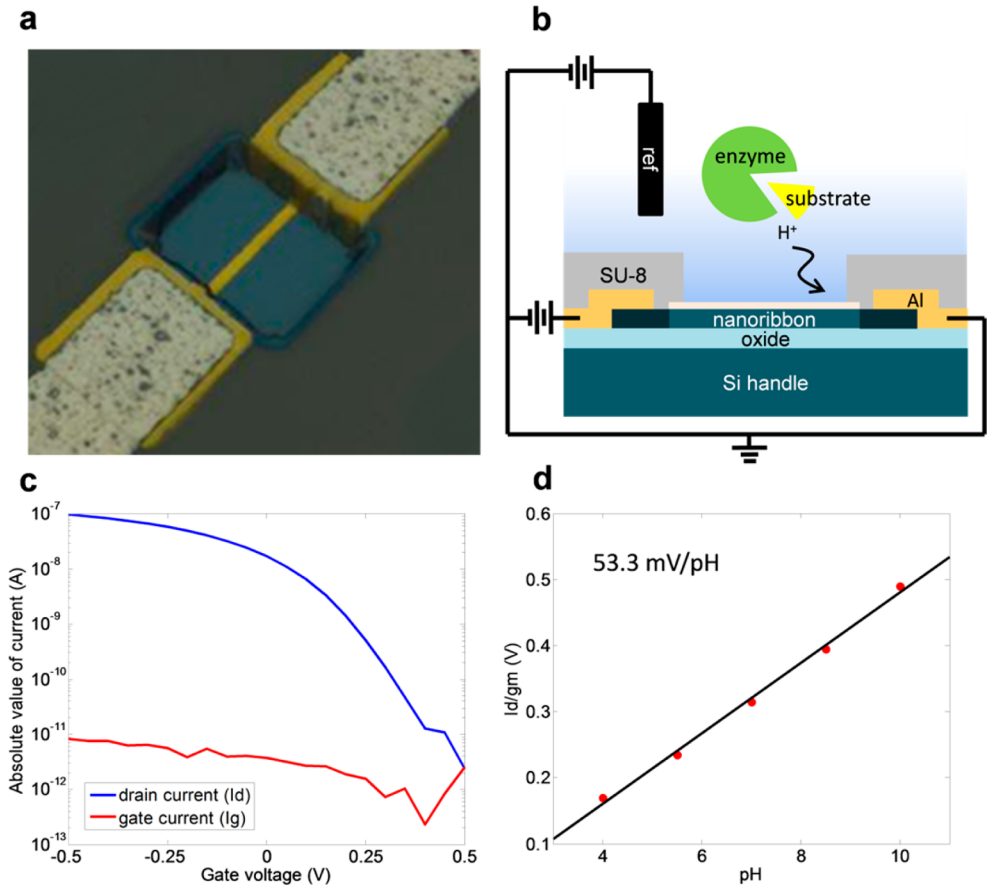

Figure 1. Typical nanoribbon device characteristics. (a) Optical image of a nanoribbon device (L = 20 μm, W = 2 μm) with a 2 μm deep via in SU-8; (b) schematic of device operation. The pH change due to enzyme (green) and substrate (yellow) interaction is measured (ref = Ag/AgCl reference electrode); (c) typical current versus gate voltage characteristic of a nanoribbon device (L = 10 μm, W = 1 μm, subthreshold swing ~80 mV/dec); (d) pH sensitivity of a nanoribbon device after BSA blocking, shown as drain current (I_d) normalized by the device transconductance (g_m).

adsorption and thus allowing device reuse. The latter is particularly important for assays where multiple reactions are to be measured using the same device.

We demonstrate the versatility of this approach through the detection of both substrate and enzyme in physiological buffers and the characterization of kinetic constants. Specifically, we show detection of urea in phosphate buffered saline (PBS) with exceptional linearity over the normal physiological range, high sensitivity detection of penicillinase in PBS and urine, and accurate analysis of the enzyme kinetics of the acetylcholinesterase−acetylcholine reaction, demonstrating that this approach can be generalized to a high-throughput platform for the detection of enzyme substrate interactions across many reaction classes.

The nanoribbon devices were fabricated using top-down lithographic techniques on 4 in. ultrathin-silicon-on-insulator (UTSOI) wafers (Soitec). The active layer as supplied is boron-doped to a carrier concentration of 10^{15}/cm^3. The wafer is RCA cleaned and the active silicon layer is thinned using an oxidation and buffered oxide etch (BOE) to a thickness of 40 nm. The areas corresponding to source and drain regions on the nanoribbons are further doped with BF_2^+ implantation at 10 keV at a dose of 2 × 10^{15} cm^2. After activation annealing, this will result in a carrier density of ~10^{19}/cm^3, which produces ohmic contacts for the source and drain. The nanoribbon dimensions are then defined in the active layer using photolithography and reactive ion etching (RIE) based on Cl_2 chemistry. After the nanoribbons are etched, the entire wafer is again RCA cleaned. Plasma-assisted atomic layer deposition (ALD) is used to deposit a 20 nm thick layer of Al_2O_3 over the entire wafer at the Cornell NanoScale Science and Technology Facility. Thermal annealing is carried out at 900 °C for 10 min to improve the dielectric−semiconductor interface. This step also serves as the source/drain activation anneal. The Al_2O_3 covering the source/drain contacts are cleared using a combination of Ar/BCl_3 milling and 10:1 BOE etching. Contact pads and interconnect metallization was done by a 200 nm thick layer of aluminum deposited by electron beam evaporation and patterned by lift-off. To further prevent leakage current from solution into the device, a 2 μm thick SU-8 layer is patterned to cover all exposed metal, opening only a small via over the nanoribbon devices to be exposed to solution. Post dicing, individual dies are wire bonded to 28 pin dual in-line (DIP) packages. A fluid reservoir is created by gluing a polypropylene tube on the surface of the chip to hold solution over the device (cut from a 200 μL pipet tip). The exposed wirebonds are sealed with epoxy (Devcon) to protect them from solution.

The devices we used varied in length between 10 and 20 μm and varied in width between 1 and 32 μm. Figure 1a shows a 3D optical profile image (Zeta-20; Zeta Instruments) of a 20 μm long and 2 μm wide ribbon. The top down process allows us to precisely and consistently define the dimensions and location of the nanoribbons, which allows for high device yield

dx.doi.org/10.1021/nl502366e | Nano Lett. 2014, 14, 5315−5322

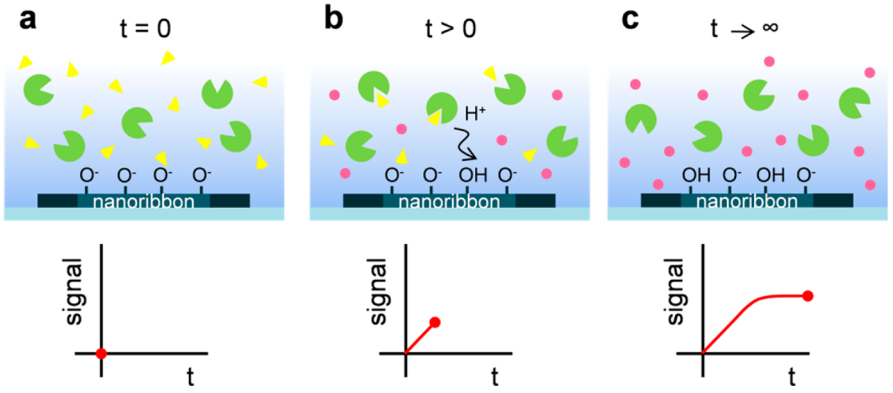

Figure 2. Overview of nanoribbon detection of enzyme (green) and substrate (yellow) interactions via pH change. (a) beginning of reaction; (b) enzymatic conversion of substrates to products with passing time; (c) reaction is completed when all substrates have been converted to products.

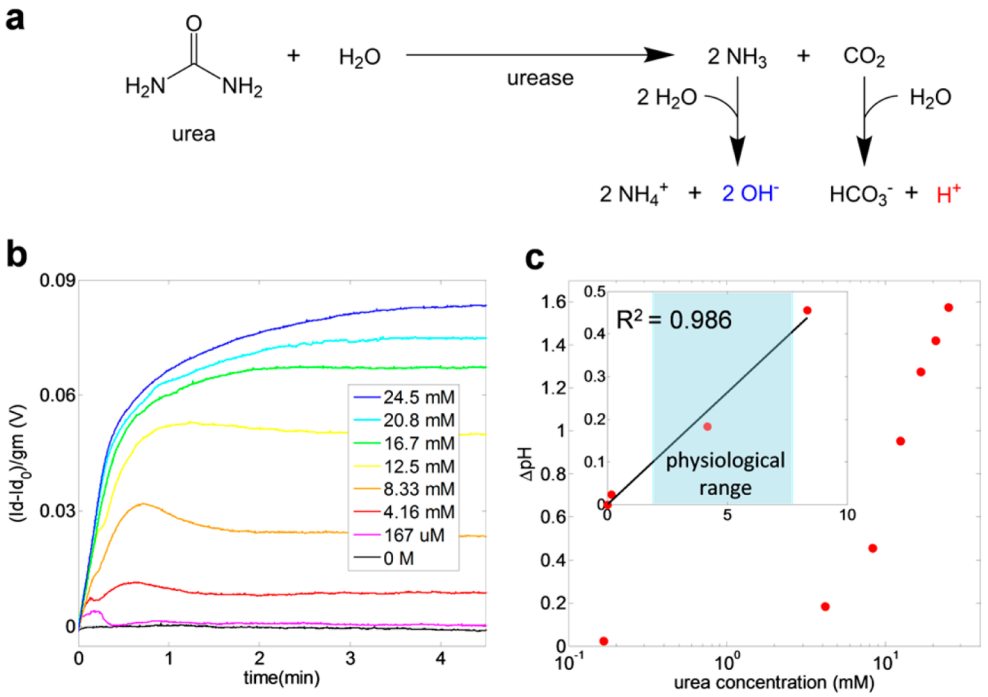

Figure 3. Detection of urea using nanoribbon pH sensors. (a) Hydrolysis of urea, catalyzed by urease, producing ammonia and carbon dioxide as products (basic groups are shown in blue, acidic groups are shown in red); (b) potential signal from urea−urease reaction versus time with different urea concentrations; (c) same data in (b) converted into a pH change using eq 2, plotted on a semilog scale. Inset shows a zoom in of the physiologically normal range (highlight in blue), plotted on a linear scale.

and repeatable electrical characteristics. A custom built buffer amplifier system is used to interrogate individual devices. The experimental setup involves the application of a drain voltage (V_d, typically 0.02 to 0.1 V) and gate voltage (V_g, typically −0.2 to −0.5 V) to set the operating point within the linear region (Figure 1b). The gate voltage is applied via a pseudoreference gate electrode made from an Ag/AgCl wire immersed in the solution contacting the device. The current from the device, I_d, is filtered (low pass, 12 dB, 10 Hz), amplified, and converted into a voltage (100 nA/V), which is read by a data acquisition (DAQ) card in real time (10 Hz sampling rate). A typical current versus gate voltage device characteristic is shown in Figure 1c.

In order to determine pH sensitivity of the nanoribbons, the devices were exposed to standard pH calibration solutions. Our devices are p-type, therefore an increase in pH corresponds to an increase in I_d, as deprotonation of siloxyl groups leads to increased negative charges on the surface. We measured the pH response of five devices randomly sampled across the wafer and obtained a pH sensitivity of 55.44 ± 2.94 mV/pH, close to the limit of 59.1 mV/pH at 25 °C. In order to suppress nonspecific adsorption of enzymes on charged surfaces (such as exposed SU-8), the entire solution reservoir was incubated with 3% bovine serum albumin (BSA; Fisher) in PBS (pH = 7.4; Gibco) for 1 h the first time each bonded die is used. The pH response was measured again after BSA treatment, and a similar pH response of 53.5 ± 3.03 mV/pH (seven devices randomly sampled) was obtained, indicating little nonspecific adsorption of proteins on the near-neutral Al_2O_3 surface. A representative pH response plot is shown in Figure 1d (53.3 mV/pH, R^2= 0.996), showing both high sensitivity and linearity after blocking.

In our experiments, enzyme and substrate are combined in solution and allowed to react (Figure 2a). The enzyme (green)

dx.doi.org/10.1021/nl502366e | Nano Lett. 2014, 14, 5315−5322

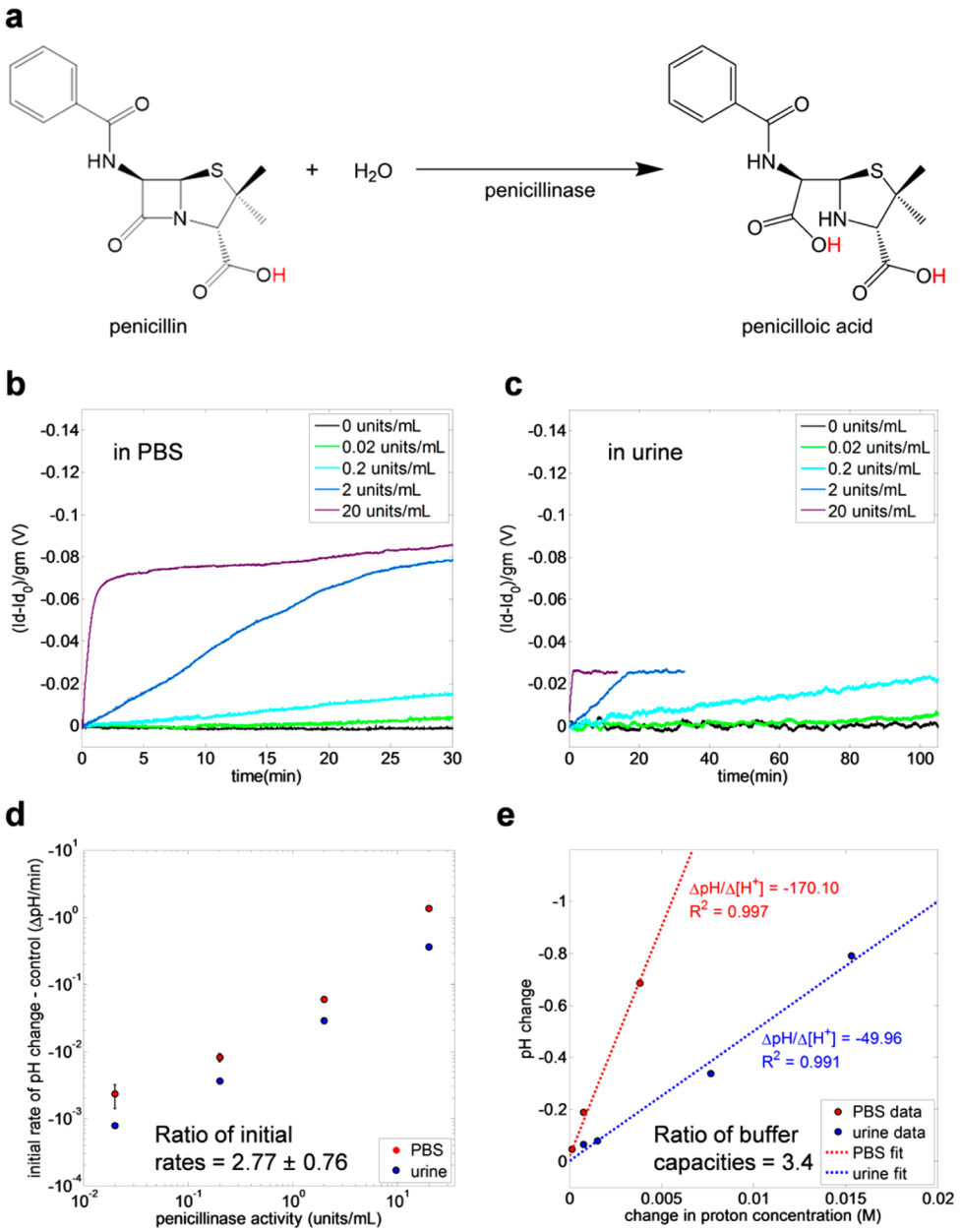

Figure 4. Detection of penicillinase enzyme activity using nanoribbon sensors. Note that increasing *y*-axis values correspond to decreasing pH. (a) Reaction between penicillin and water, catalyzed by penicillinase, producing penicilloic acid as product (acidic groups are shown in red); (b) potential signal from penicillin−penicillinase reaction in PBS versus time with different penicillinase activities; (c) potential signal from pencillin−penicillinase reaction in urine versus time with different penicillinase activities; (d) initial response rates from (b,c) converted into a pH change rate using eq 2; (e) titration data of HCl in PBS (red) and urine (blue). Linear fits to the data show the ratio of the buffering capacities (3.4) of the two samples.

catalyzes the conversion of substrates (yellow) into products (pink), which can alter the pH of its environment in the process (Figure 2b). The change in pH can be measured by the nanoribbon in solution in real time and is reflected in the change in I_d through the device. As the reaction goes to completion, all of the available substrates are converted into products, hence the signal saturates to a stable value (Figure 2c).

We use the urea−urease reaction as a model system to demonstrate the ability of silicon nanoribbons to carry out substrate detection. Urea is an important compound in metabolic processes and its concentration in physiological solutions, such as blood or urine, is an important diagnostic measure of renal, liver, heart, and other diseases.[26−28] The normal level of urea in human serum is 1.9−7.7 mM,[29] and elevated levels are indicative of renal damage.

Urease catalyzes the hydrolysis of urea to ammonia and carbon dioxide (Figure 3a). The ammonia released into solution is spontaneously protonated to ammonium, while the CO_2 is changed to bicarbonate. Because twice as much NH_3 is released compared to CO_2, the pH increases as the reaction proceeds.

The detection of urea is demonstrated using different concentrations of urea (Sigma) diluted into PBS. One hundred microliters of the urea solution was added to the sensing reservoir and a stable baseline was obtained. Fifty microliters of

dx.doi.org/10.1021/nl502366e | *Nano Lett.* 2014, 14, 5315−5322

a high concentration solution (4.5 mg/mL) of urease from *Canavalia ensiformis* (EC 3.5.1.5; Sigma) was subsequently added by pipetting, and the response was monitored. Time = 0 was defined after recovery to baseline after a brief (~few seconds) transient due to fluid injection. The initial current at time = 0 (I_{d0}) was subtracted from the measured current for each concentration (I_d), and the difference was divided by the transconductance in the linear regime (g_m); that is

$$\frac{I_d - I_{d0}}{g_m} \quad (1)$$

This metric is independent of variations in device geometry and depends only on the surface potential.[30] The results are plotted in Figure 3b. The small peak observed near the start of the reaction is likely a result of the faster ammonia protonation compared to the biocarbonate formation. As the reaction proceeds, the signal approaches a stable value. The difference between this limiting value and the control value can be related to the final pH change in solution (Figure 3c) using

$$\Delta pH = \frac{I_d - I_{d0}}{g_m \gamma} \quad (2)$$

where γ is the pH sensitivity of the device (53.5 mV/pH). Despite the strong buffering capacity of the PBS, urea detection can be achieved with a starting urea concentration as low as 167 μM (ΔpH = 0.023). This limit can be further decreased by adding a smaller volume of concentrated enzyme solution to reduce signal dilution. The normal range for blood urea is colored blue in Figure 3c.

This method is insensitive to variations in enzyme concentration and small variations in enzyme activity due to changes in pH, as the metric of interest is the final pH change in comparison to the control. Over the expected blood urea concentration range, the signal is linear (R^2 = 0.986; Figure 3c, inset). At extremely high urea concentrations, the signal tends toward saturation, most likely because either the pH or NH_4^+ concentration has changed so much that the activity of the enzyme is significantly inhibited,[31,32] and therefore substrates were not exhausted. In applications where a larger dynamic range is desired, an additional feedback unit can be used to readjust the pH of the solution back to the optimal point throughout the reaction.[33]

In addition to substrate detection, another appealing feature of the approach is the ability to carry out enzyme activity quantification. We show that by using the nanoribbon as a pH sensor without functionalization, we can easily and reliably measure enzyme activity to very low levels. To demonstrate this, we use the nanoribbons to detect penicillinase, an enzyme that hydrolyzes penicillin G. Despite the rapid development of penicillin resistance in bacteria with the introduction of penicillin in the 1940s,[34] penicillin remains an important antibiotic used in the medical industry today, as many strains of bacteria are still susceptible. Therefore, it is critical to be able to measure penicillin resistance, which is frequently attributed to the presence of penicillinase.[34] Current methods of penicillinase detection involve the use of a penicillin disk,[35] which lacks sensitivity. The hydrolysis of penicillin G releases a proton and lowers the pH of the solution as shown in Figure 4a. By mixing the enzyme with a high concentration of penicillin, we can measure the rate of pH decrease and thus deduce the enzyme concentration.

We varied the concentration of penicillinase from *Bacillus cereus* (EC 3.5.2.6; Sigma) from 0 to 20 units/mL in PBS (a unit of enzyme is defined as the amount of enzyme required to catalyze 1 μmol of substrate at optimal pH and temperature), and added 100 μL of the enzyme solution into the cup to achieve a steady baseline. Fifty microliters of a high concentration (12.8 mg/mL) of penicillin G (Sigma) was then added and mixed by pipetting. ΔI_d was monitored for 30 min from the moment the mixing was complete (Figure 4b) and subsequently converted to the equivalent pH change rate using eq 2 (Figure 4d, red). Each data point was repeated 5 times, the penicillinase-free control was repeated 3 times, and the mean control rate was subtracted from the rate measured for each concentration. The standard errors of the mean are shown for each PBS data point in Figure 4d. After only a few minutes of reaction time, the detection limit can reach as low as 0.2 units/mL, and within 30 min the detection limit can reach 0.02 units/mL with the potential of becoming lower with even longer incubation time. Al_2O_3 is known to have low drift (<1 mV/h, equivalent to <0.02 pH units/h), allowing long-term measurements to be taken.[25] For this sample of penicillinase, 0.02 units/mL is equivalent to an enzyme concentration of 300 pM.

Penicillin-resistant urinary tract infections (UTIs) are a common condition,[36] and blood sepsis patients can show bacteria in urine.[37] Therefore, we addressed the question of whether we can achieve effective penicillinase detection in urine. A urine sample (pH 7–7.5) was collected, filtered through a 0.22 μm pore syringe filter, and kept at 4 °C until use. Experiments were conducted within 48 h of sample collection. We conducted the same penicillinase sensing experiment in urine as we did for PBS (Figure 4c). We found that the initial rate of signal change in urine was considerably slower than that of PBS, and we had to monitor the reaction over a longer time period in order to maintain the same detection limit. As a result, we were able to detect 0.02 units/mL of penicillinase in urine in just under 2 h. The initial rate of change in the pH as a function of penicillinase activity is shown in Figure 4d (blue). We found that the ratio between the rates of pH change in PBS and urine is 2.77 ± 0.76. It is also worth noting that as the signal saturates due to substrate depletion, the saturated signal for PBS is higher than that of urine by approximately the same ratio, despite the substrate concentration being the same in both sets of experiments. This indicates that the difference between urine and PBS is mainly a result of the higher buffering capacity of urine, caused by the presence of phosphate, ammonia, various organic solutes, and proteins. To test this, we measured the buffering capacity of these two sample solutions by generating a pH titration curve. We titrated PBS and urine with HCl over the nanoribbons and measured the pH response. Two microliters of HCl solution of different concentrations was added to 150 μL of the sample buffer, and the pH response was extracted and plotted against the final change in proton concentration (Figure 4e). Because of buffering, small changes in proton concentrations near the buffers' pK lead to a linear change in pH. The data within 1 unit of pH change from original was fit with a straight line, and the slope is extracted as the buffering capacity. It was found that the buffering capacity of urine close to the original pH of the solution was approximately 3.4 times that of PBS (Figure 4e), consistent with the difference we observed between the rates and signals of the PBS versus urine measurements (Figure 4d). This is an important calibration method, as an issue with pH-

dx.doi.org/10.1021/nl502366e | *Nano Lett.* 2014, 14, 5315–5322

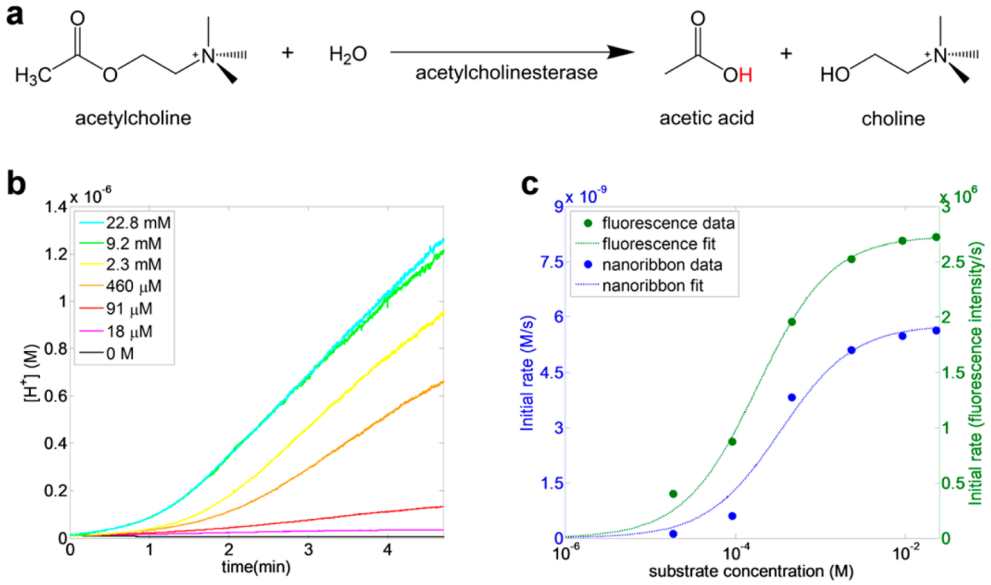

Figure 5. Analysis of acetylcholinesterase enzyme kinetics using nanoribbon sensors. (a) Reaction between acetylcholine and water, catalyzed by acetylcholinesterase, producing acetic acid and choline as products (acidic groups are shown in red); (b) nanoribbon signal from acetylcholine–acetylcholinesterase reaction converted into its equivalent proton concentration over time; and (c) Michaelis–Menten fits to nanoribbon and fluorescence data.

based detection is the variability of buffering capacity between different biological samples and thus the difficulty of generalizing the method of pH detection across all types of solutions. Thus, this challenge can be easily overcome by generating a titration curve in the buffer of interest prior to running the enzymatic reaction and will allow for the estimation of enzyme activity in complex solutions or solutions differing in buffer capacity.

Nanoribbon sensors have the additional advantage of real time signal transduction, which permits the extraction of kinetic constants of the system.[30] To demonstrate this application for enzyme–substrate pairs, we use the system of acetylcholine and acetylcholinesterase. Acetylcholinesterase controls the half-life of acetylcholine, a crucial neurotransmitter. The ability to probe the interaction between acetylcholine and its esterase may provide valuable insight into the termination of synaptic transmission. From the reaction of acetylcholine and acetylcholinesterase (Figure 5a), one can see how this pH detection method can be generalized to probe all reactions catalyzed by esterases, as the products will always yield a carboxylic acid group and an alcohol group. The carboxylic acid deprotonates at neutral pH, thus increasing the acidity of the solution. One of the best-known models of enzyme kinetics is based on the Michaelis–Menten equation

$$v = V_{max}\frac{[S]}{K_m + [S]} \tag{3}$$

where v is the initial rate of product generation, V_{max} is the rate of product generation at saturating substrate concentration, $[S]$ is the initial substrate concentration, and K_m is the Michaelis–Menten constant, equivalent to $[S]$ at which v reaches $(1/2)$ V_{max}. K_m is an important kinetic value describing the affinity between the enzyme–substrate pair and can be extracted by measuring initial reaction rates as a function of substrate concentration.

To monitor the kinetics of the reactions and determine K_m we carried out the reaction in water, so that initial reaction velocities can be easily determined and the pH changes will remain unbuffered. We compared the results of our method against spectrophotometric fluorescence detection, which is a commonly accepted method of extracting K_m. A series of experiments was conducted using each method at room temperature, where the enzyme concentration was held constant (1.28 units/mL) and the substrate concentration was varied. The same batch of acetylcholinesterase (EC 3.1.1.7; Life Technologies) and acetylcholine (Life Technologies) were used for each experiment. In the nanoribbon assay, acetylcholine and acetylcholinesterase from *Electrophorus electricus* were mixed in molecular grade water (supplemented with 150 mM NaCl and pH adjusted to 8; Sigma) in a fluid reservoir over the nanoribbon. The pH change was monitored over time. In the fluorescence assay (Life Technologies), the same acetylcholine and acetylcholinesterase were mixed together in a 96 well plate in 50 mM Tris-HCl, pH = 8.0. The choline product from the reaction was oxidized by choline oxidase to produce H_2O_2, which in the presence of horseradish peroxidase reacts with Amplex Red to yield resorufin, a highly fluorescent molecule. Fluorescence was measured over time using the SpectraMax Paradigm microplate reader (Molecular Devices) at an excitation of 555 nm and emission of 595 nm.

The nanoribbon signal was converted to ΔpH versus time using eq 2, then to proton concentration $[H^+]$ vs time using

$$[H^+] = 10^{-(8+\Delta pH)} \tag{4}$$

with time = 0 being the moment the transients from mixing have subsided (Figure 5b). The initial 1–2 min exhibited significant nonlinearity because of slight buffering from the proteins in the system, so initial reaction rates were extracted from the slopes in the linear regime. In the fluorescence experiment, the initial slope was extracted using SoftMax Pro Software (Molecular Devices) in the linear range of the assay. We fitted the Michaelis–Menten equation to the initial reaction rate versus substrate concentration data from both methods, and we show both on the same graph (Figure 5c). K_m values of

dx.doi.org/10.1021/nl502366e | *Nano Lett.* 2014, 14, 5315–5322

$(3.33 \pm 0.89) \times 10^{-4}$ M and $(1.79 \pm 0.19) \times 10^{-4}$ M were obtained on the nanoribbon and spectrophotometer, respectively (Table 1). The reported value of K_m for acetylcholinesterase from *Electrophorus electricus* reacting with acetylcholine is 7.39×10^{-5} M, using a matrix-assisted laser desorption/ionization Fourier transform mass spectrometry (MALDI-FTMS) based assay.[38] The K_m value obtained on the nanoribbon is very similar to that obtained using fluorescence, and both values are in reasonable agreement with previously reported value in literature considering sample variations, showing that nanoribbons are a viable method of probing enzyme−substrate affinity.

Table 1. Comparison of K_m Values Obtained via Different Methods

method	K_m (M)	R^2
nanoribbon	$(3.33 \pm 0.89) \times 10^{-4}$	0.973
fluorescence	$(1.79 \pm 0.19) \times 10^{-4}$	0.994
literature (MALDI-FTMS[38])	7.39×10^{-5}	0.995

In conclusion, we have shown that properly designed electronic FETs can be used as sensitive and reliable devices for measuring enzyme−substrate interactions. Substrate and enzyme concentration can be detected using pH change, even in highly buffered solutions. For substrate detection using urea as a model system, we have demonstrated a detection limit of less than 200 μM in PBS. We have also demonstrated an enzyme detection limit of 0.02 units/mL for the penicillin−penicillinase model system in PBS and urine, which we note is a general detection limit applicable to other enzymatic reactions that produce a proton. We also showed that enzyme kinetics can be analyzed to accurately determine the kinetic constant K_m, and we validated our technique against fluorescence spectroscopy. Our electronic method is readily generalized to many unrelated classes of substrates and enzymes. An additional advantage of our method of enzyme detection is that it does not require the use of high-affinity antibodies, which have limited availability for many enzymes. Our approach also allows the incorporation of on-chip control devices coated with a material with subdued pH response, such organosilanes[39] or polymers,[40] so that differential measurements can be taken.

We believe that this method can be adapted to a simple, compact, inexpensive, and sensitive platform for high-throughput detection of different enzyme activities and substrate concentrations. The small size of our devices offer potential for future scaling to much smaller volumes as well as potential integration with other on-chip signal processing components. Applications of our method include, but are not limited to, high-throughput in vitro and in vivo mutant and RNA-interference screening to identify novel metabolic regulators and comprehensive profiling of patient tissues and fluids for personalized disease diagnosis and therapeutic monitoring.

AUTHOR INFORMATION

Corresponding Author

*E-mail: mark.reed@yale.edu.

Present Address

(N.K.R.) California NanoSystems Institute at UC Santa Barbara, University of California Santa Barbara, Santa Barbara, CA, 93106, U.S.A.

Author Contributions

The manuscript was written through contributions of all authors. All authors have given approval to the final version of the manuscript.

Notes

The authors declare no competing financial interest.

ACKNOWLEDGMENTS

This work was supported in part by U.S. Army Research Office and Air Force Research Laboratory, under contract/grant number MURI W911NF-11-1-0024, and Air Force Research Laboratory under UES Subcontract Number S-875-001-007, and Natural Sciences and Engineering Research Council of Canada (NSERC) graduate fellowships (L.M., I.A.D.). Facilities used were supported by Yale Institute for Nanoscience and Quantum Engineering and NSF MRSEC DMR 1119826. We thank V. Genova at Cornell NanoScale Science & Technology Facility and the staff at Yale School of Engineering & Applied Science Cleanroom (M. Power, C. Tillinghast, J. Agresta) for device fabrication assistance. We also thank X. Duan, M. Weber, S. Yosinski, X. Li, and Z. Kobos for helpful discussions.

REFERENCES

(1) Goddard, J.-P.; Reymond, J.-L. *Trends Biotechnol.* **2004**, *22*, 363−370.

(2) Zhang, M.; Karra, S.; Gorski, W. *Anal. Chem.* **2013**, *85*, 6026−6032.

(3) Wallace, T. C.; Coughlin, R. W. *Anal. Biochem.* **1977**, *80*, 133−144.

(4) Kroger, S.; Setford, S. J.; Turner, A. P. *Biotechnol. Technol.* **1998**, *12*, 123−127.

(5) Schomburg, I.; Chang, A.; Placzek, S.; Söhngen, C.; Rother, M.; Lang, M.; Munaretto, C.; Ulas, S.; Stelzer, M.; Grote, A. *Nucleic Acids Res.* **2013**, *41*, D764−D772.

(6) Janata, J.; Moss, S. D. *Biomed. Eng.* **1976**, *11*, 241−245.

(7) Danielsson, B.; Lundström, I.; Mosbach, K.; Stiblert, L. *Anal. Lett.* **1979**, *12*, 1189−1199.

(8) Boubriak, O.; Soldatkin, A.; Starodub, N.; Sandrovsky, A.; El'skaya, A. *Sens. Actuators, B* **1995**, *27*, 429−431.

(9) Pijanowska, D. G.; Torbicz, W. *Sens. Actuators, B* **1997**, *44*, 370−376.

(10) Alegret, S.; Bartroli, J.; Jimenez, C.; Martinez-Fabregas, E.; Martorell, D.; Valdes-Perezgasga, F. *Sens. Actuators, B* **1993**, *16*, 453−457.

(11) Soldatkin, A. P.; Montoriol, J.; Sant, W.; Martelet, C.; Jaffrezic-Renault, N. *Talanta* **2002**, *58*, 351−357.

(12) Sant, W.; Pourciel-Gouzy, M.; Launay, J.; Do Conto, T.; Colin, R.; Martinez, A.; Temple-Boyer, P. *Sens. Actuators, B* **2004**, *103*, 260−264.

(13) Dzyadevich, S. V.; Korpan, Y. I.; Arkhipova, V. N.; Alesina, M. Y.; Martelet, C.; El'Skaya, A. V.; Soldatkin, A. P. *Biosens. Bioelectron.* **1999**, *14*, 283−287.

(14) Luo, X.-L.; Xu, J.-J.; Zhao, W.; Chen, H.-Y. *Biosens. Bioelectron.* **2004**, *19*, 1295−1300.

(15) Soldatkin, A.; El'Skaya, A.; Shul'ga, A.; Netchiporouk, L.; Nyamsi Hendji, A.; Jaffrezic-Renault, N.; Martelet, C. *Anal. Chim. Acta* **1993**, *283*, 695−701.

(16) Caras, S.; Janata, J. *Anal. Chem.* **1980**, *52*, 1935−1937.

(17) Poghossian, A.; Schöning, M.; Schroth, P.; Simonis, A.; Lüth, H. *Sens. Actuators, B* **2001**, *76*, 519−526.

(18) Chi, L.-L.; Yin, L.-T.; Chou, J.-C.; Chung, W.-Y.; Sun, T.-P.; Hsiung, K.-P.; Hsiung, S.-K. *Sens. Actuators, B* **2000**, *71*, 68−72.

(19) Hai, A.; Ben-Haim, D.; Korbakov, N.; Cohen, A.; Shappir, J.; Oren, R.; Spira, M. E.; Yitzchaik, S. *Biosens. Bioelectron.* **2006**, *22*, 605−612.

(20) van der Schoot, B. H.; Bergveld, P. *Biosensors* **1988**, *3*, 161−186.

(21) Rodrigues, R. C.; Ortiz, C.; Berenguer-Murcia, Á.; Torres, R.; Fernández-Lafuente, R. *Chem. Soc. Rev.* **2013**, *42*, 6290−6307.
(22) Stern, E.; Vacic, A.; Rajan, N. K.; Criscione, J. M.; Park, J.; Ilic, B. R.; Mooney, D. J.; Reed, M. A.; Fahmy, T. M. *Nat. Nanotechnol.* **2009**, *5*, 138−142.
(23) Chen, S.; Bomer, J. G.; Carlen, E. T.; van den Berg, A. *Nano Lett.* **2011**, *11*, 2334−2341.
(24) Reddy, B., Jr; Dorvel, B. R.; Go, J.; Nair, P. R.; Elibol, O. H.; Credo, G. M.; Daniels, J. S.; Chow, E. K.; Su, X.; Varma, M. *Biomed. Microdevices* **2011**, *13*, 335−344.
(25) Bae, T.-E.; Jang, H.-J.; Yang, J.-H.; Cho, W.-J. *ACS Appl. Mater. Interfaces* **2013**, *5*, 5214−5218.
(26) Aronson, D.; Mittleman, M. A.; Burger, A. J. *Am. J. Med.* **2004**, *116*, 466−473.
(27) Carvounis, C. P.; Nisar, S.; Guro-Razuman, S. *Kidney Int.* **2002**, *62*, 2223−2229.
(28) Hosten, A. O. BUN and Creatinine. In *Clinical Methods: The History, Physical, and Laboratory Examinations*, 3rd ed.; Walker, H. K., Hall, W. D., Hurst, J. W., Eds.; Butterworths: Boston, 1990; pp 874−878.
(29) MacKay, E. M.; MacKay, L. L. *J. Clin. Invest.* **1927**, *4*, 295−306.
(30) Duan, X.; Li, Y.; Rajan, N. K.; Routenberg, D. A.; Modis, Y.; Reed, M. A. *Nat. Nanotechnol.* **2012**, *7*, 401−407.
(31) Kay, W. W.; Reid, M. A. H. *Biochem. J.* **1934**, *28*, 1798.
(32) Cheng, K.-J.; Wallace, R. *Br. J. Nutr.* **1979**, *42*, 553−557.
(33) van der Schoot, B. H.; Voorthuyzen, H.; Bergveld, P. *Sens. Actuators, B* **1990**, *1*, 546−549.
(34) Davies, J.; Davies, D. *Microbiol. Mol. Biol. Rev.* **2010**, *74*, 417−433.
(35) Hodge, W.; Ciak, J.; Tramont, E. C. *J. Clin. Microbiol.* **1978**, *7*, 102−103.
(36) Pallett, A.; Hand, K. *J. Antimicrob. Chemother.* **2010**, *65*, iii25−iii33.
(37) Lee, B. K.; Crossley, K.; Gerding, D. N. *Am. J. Med.* **1978**, *65*, 303−306.
(38) Xu, Z.; Yao, S.; Wei, Y.; Zhou, J.; Zhang, L.; Wang, C.; Guo, Y. *J. Am. Soc. Mass. Spectrom.* **2008**, *19*, 1849−1855.
(39) Tarasov, A.; Wipf, M.; Bedner, K.; Kurz, J.; Fu, W.; Guzenko, V.; Knopfmacher, O.; Stoop, R.; Calame, M.; Schönenberger, C. *Langmuir* **2012**, *28*, 9899−9905.
(40) Errachid, A.; Bausells, J.; Jaffrezic-Renault, N. *Sens. Actuators, B* **1999**, *60*, 43−48.